

Traveling wave solutions for non-Newtonian foam flow in porous media

Wesley da Silva Pereira, wesley.pereira@ucdenver.edu^{1,2} and
Grigori Chapiro, grigori@ice.ufjf.br¹

¹Department of Mathematics, Federal University of Juiz de Fora,
Rua José Lourenço Kelmer, s/n - São Pedro, Juiz de Fora,
36036900, MG, BR

²Department of Mathematical and Statistical Sciences, University
of Colorado Denver, 1201 Larimer Street, Denver, 80204, CO, US

October 3, 2022

Abstract

The injection and in-situ generation of foam in porous media successfully control gas mobility and improve the fluids' sweep efficiency inside porous media. Mathematical models describing this problem use two phases, foamed gas and fluid, and usually have a term for foam generation and destruction. Moreover, the non-Newtonian foam behavior is frequently modeled using the Hirasaki and Lawson's formula for foamed gas viscosity. In this paper, we detail how the traveling wave analysis can be used to estimate the propagation profiles and velocity for a range of non-Newtonian foam models in porous media at constant total superficial flow velocity. We reformulate Hirasaki and Lawson's formula in an explicit form allowing us to find traveling wave solutions for the non-Newtonian Linear Kinetic model. Comparing the solution with the one for the Newtonian version, allows us to analyze qualitatively and quantitatively the rheology of the foam flow in porous media.

Funding

This research was carried out in association with the ongoing R&D project registered as ANP 20715-9, "Modelagem matemática e computacional de injeção de espuma usada em recuperação avançada de petróleo" (Universidade Federal de Juiz de Fora (UFJF) / Shell Brasil / ANP) - Mathematical and computational modeling of foam injection as an enhanced oil recovery technique applied to Brazil pre-salt reservoirs, sponsored by Shell Brasil under the ANP R&D levy as "Compromisso de Investimentos com Pesquisa e Desenvolvimento". This project is carried out in partnership

with Petrobras. The author G. Chapiro was supported in part by CNPq grant 303245/2019-0.

1 Introduction

One technique to control gas mobility and improve fluid sweep efficiency in a porous medium consists of injecting foaming agents, e.g., surfactants and nanoparticles, in aqueous solutions that create bubbles in the gas phase. Several studies point out the favorable application of this method in enhanced oil recovery, e.g., (Casteel and Djabbarah, 1988; Grassia et al., 2014), acid diversion during matrix stimulation, e.g., (Behenna, 1995), and contaminated aquifer remediation, e.g., (Burman and Hall, 1986).

The behavior of foam is frequently reported as shear-thinning (Fernø et al., 2016; Heller and Kuntamukkula, 1987; Marsden and Khan, 1966; Zitha, 2006), which means that its apparent viscosity decreases with increased shear stress. Hirasaki and Lawson (1985) derived a shear-thinning expression for the apparent viscosity of foam flowing in capillary tubes and validated it through laboratory experiments. This non-Newtonian formula is consistent with the classical result of Bretherton (1961) using isolated bubbles and has application in several foam propagation models, e.g., (Izadi and Kam, 2019; Kam, 2008; Kovscek et al., 1995; Simjoo and Zitha, 2015). Hirasaki and Lawson's expression implicitly defines the apparent gas viscosity as it depends on the gas velocity, and the gas velocity depends on the viscosity. Other works report that foam behaves as a Newtonian fluid for particular regimes. For example, foam flow can be classified as Newtonian under nearly-constant capillary pressure during steady radial flow (Rossen, 1991). Following this idea, some models consider foam flow to be a Newtonian fluid (Ashoori et al., 2011; Lozano et al., 2021) and present results compatible with experimental data (Zavala et al., 2021). Hirasaki and Lawson's formula is so important that numerous papers investigate the foam flow in porous media only focusing on the apparent viscosity (or, equivalently, the mobility reduction factor).

The studies reported above motivate the current discussion on when to consider non-Newtonian behavior of the foam flow. Vassenden and Holt (1998) present and validate a model for the transition of foam flow behavior from Newtonian to shear-thinning according to the gas flow rate. Alvarez et al. (2001) conclude the foam behavior is shear-thinning in the low-quality regime and shear-thickening in high-quality regimes. Rossen (1991) highlights the change from Newtonian to non-Newtonian behavior of uniform texture foam for changing capillary pressure.

One may find several predictive mathematical models in the literature aiming to represent foam propagation inside porous media. Local Equilibrium (LE) foam models use algebraic expressions to compute the foam texture. However, LE models can be inadequate when strong foam generation is not certain (Kam et al., 2007). Mechanistic foam models, introduced by Falls et al. (1988); Patzek (1988), describe the foam texture dynamically using partial differential equations (PDE). They have the unique potential to describe both transient and stationary conditions for foam flow as they track the foam texture in space and time (Eide et al., 2020). Many works

report mechanistic models to match laboratory experiments successfully, e.g., in (Kovscek et al., 1995; Kam, 2008; Simjoo and Zitha, 2015). Besides that, some authors prefer these models when extracting analytical estimates of the foam flow, e.g., (Almajid et al., 2019; Eide et al., 2020; Simjoo and Zitha, 2015). Moreover, several works suggest that, after a transient stage, foam travels inside the porous media under invariant water saturation profiles, e.g., (de Vries and Wit, 1990; Ettinger and Radke, 1992). One strategy to obtain solution profiles, employed in (Izadi and Kam, 2019; Kam, 2008; Simjoo and Zitha, 2015), consists of disregarding the capillary pressure gradient in each phase’s superficial velocity and applying the classical method of characteristics. Another strategy consists of seeking traveling waves solutions, which are profiles invariant to translation in space (Volpert et al., 2000). They are especially suited for analyzing nonlinear wave propagation problems at constant speed. Ashoori et al. (2011); Lozano et al. (2021) used this procedure to find traveling wave solutions for Newtonian foam models at fixed total superficial velocity. Ashoori et al. (2011) also find traveling waves for the model from Kam (2008) which does not consider capillary pressure derivatives.

The present work shows how to compute traveling wave solutions that connect two equilibrium states of a generic mechanistic non-Newtonian foam model that consider capillary pressure derivatives. We assume the total superficial velocity is fixed, which is the case of predominant rectilinear flow. The non-Newtonian foamed gas viscosity is modeled by the Hirasaki and Lawson’s formula. We rewrite this formula in terms of water saturation, foam texture and total superficial velocity to avoid the direct dependency on the gas superficial velocity. The traveling wave profiles serve as basis to compare a linear kinetic foam model using Newtonian and non-Newtonian gas viscosity expressions.

We organize this paper as follows. Section 2 presents the general population-based foam model. Section 3 shows the Hirasaki and Lawson apparent gas viscosity and its reformulated version. Section 4 presents the procedure for obtaining traveling wave solutions for the non-Newtonian foam flow model. Section 5 applies the procedure to a linear kinetics model, and use the traveling wave profiles to compare Newtonian and non-Newtonian models. Section 6 presents the discussions and conclusions.

2 The population-balance foam model

Consider the two-phase flow of gas-water solution with foaming agents in a porous medium, where the flow occurs only in one direction, and all fluids are incompressible. The last assumption is undesirable but necessary for the mathematical analysis performed in this paper. The process is modeled by the mass balance of each phase i as

$$\frac{\partial(\phi S_i)}{\partial t} + \frac{\partial u_i}{\partial x} = 0, \quad i \in \{w, g\}, \quad (1)$$

where t is the time variable, x is the space variable, ϕ is the porosity, S_i and u_i are the saturation and superficial velocity of the phase i . The

subscript ‘ w ’ represents the aqueous phase and ‘ g ’ represents the gas phase. The phase superficial velocities satisfy the generalized Darcy’s laws (Chen and Ewing, 1997)

$$u_w = f_w \left(u + \lambda_g K \frac{\partial P_c}{\partial x} \right), \quad u_g = f_g \left(u - \lambda_w K \frac{\partial P_c}{\partial x} \right), \quad (2)$$

with fractional fluxes f_i and phase mobilities λ_i given by

$$f_i := \frac{\lambda_i}{\lambda_w + \lambda_g}, \quad \lambda_i := \frac{k_{ri}}{\mu_i}, \quad i \in \{w, g\}, \quad (3)$$

where K is the permeability, $u = u_w + u_g$ is the (constant) total superficial velocity, P_c is the capillary pressure, and for each phase i , k_{ri} is the relative permeability, and μ_i is the apparent phase viscosity. The balance of foam texture n_f in the gas phase is

$$\frac{\partial(\phi S_g n_f)}{\partial t} + \frac{\partial(n_f u_g)}{\partial x} = \phi S_g R, \quad (4)$$

where $R := r_g - r_c$, and r_g and r_c are the rates of generation and coalescence of foam, respectively. It is useful to define the dimensionless foam texture (n_D) as follows

$$n_D := \frac{n_f}{n_{\max}}, \quad (5)$$

where n_{\max} is the reference foam texture.

Some auxiliary physical quantities are equally important in this work. We define the effective water saturation (S_{we}), with values in $[0,1]$, as

$$S_{we} := \frac{S_w - S_{wc}}{1 - S_{wc} - S_{gr}}, \quad (6)$$

where S_{wc} is the connate water saturation, and S_{gr} is the residual gas saturation. The total apparent viscosity (μ_{app}) is

$$\mu_{app} := \frac{1}{\lambda_w + \lambda_g}, \quad (7)$$

and the mobility reduction factor (MRF) is

$$MRF := \frac{\mu_g}{\mu_g^0}. \quad (8)$$

To avoid problems in the nomenclature, we emphasize using the word “total” when referring to the apparent viscosity μ_{app} . Note that the apparent total viscosity represents the equivalent viscosity of the fluid system in the following Darcy’s law

$$u = -\frac{K}{\mu_{app}} \nabla P, \quad (9)$$

where P is the global pressure (Antontsev, 1972). Finally, the phase- i interstitial velocity is

$$v_i := \frac{|u_i|}{\phi S_i}, \quad i \in \{w, g\}. \quad (10)$$

It is worth mentioning that several models exist that state P_c depending exclusively on the fluid phase saturation, and many of them are based on the classical works of Corey (1954); Brooks and Corey (1966); van Genuchten (1980). The relative permeabilities k_{rw} and k_{rg} are either derived directly from the capillary pressure or fitted experimentally (see (Li and Horne, 2006) and references therein). Foam generation and coalescence expressions r_g and r_c are either inspired on microscopic mechanisms (Kam, 2008; Kovscek et al., 1995), based on macroscopic observations (Ashoori et al., 2011; Simjoo and Zitha, 2015), or fitted using laboratory experiments (Thorat and Bruining, 2016). We postpone the definitions of the expressions $k_{rw}(S_w)$, $k_{rg}(S_w)$, $r_g(S_w, n_D, u_w)$, $r_c(S_w, n_D, u_w)$, and $P_c(S_w)$ to Section 5. Section 3 presents the formulas for the apparent gas viscosity (μ_g).

Some mechanistic (population-based) models use an expression for LE foam texture, n_D^{LE} , that naturally arises from the restriction $R = 0$. For example:

- The model from Simjoo and Zitha (2015) uses a constant value n_D^{LE} , which is compatible with laboratory experiments.
- In (Ashoori et al., 2011), $R = 0$ if and only if $n_D = n_D^{LE}(S_w) = \tanh(400(S_w - 0.37))$, which approximates the Heaviside step function.
- In (Chen et al., 2010), n_D^{LE} is the only real solution of

$$(n_D^{LE})^3 + \frac{k_{-1}v_g^{2/3}}{k_1^0v_w}n_D^{LE} - 1 = 0, \quad (11)$$

where k_{-1} and k_1^0 are positive coefficients possibly depending on S_w .

In the examples above, $0 \leq n_D^{LE} \leq 1$. The expression n_D^{LE} from Kovscek et al. (1995) can be also written as a function of S_w , v_w and v_g but it is not constrained to the interval $[0, 1]$. In (Kam, 2008), n_D^{LE} is also not constrained to the interval $[0, 1]$ and it is a function of S_w and ∇P (See (Ashoori et al., 2011) for a traveling wave analysis of the model in (Kam, 2008)).

Remark. Some models make a distinction between trapped and flowing foam phases, e.g., (Izadi and Kam, 2019; Kovscek et al., 1995; Kharabaf and Yortsos, 1998). Other studies report the importance of understanding the gas trapping mechanism to model foam flow in porous media (Almajid et al., 2019; Jones et al., 2018). Simjoo and Zitha (2015) observe no trapping, arguing that foam could be moving slowly. On top of that, it is still not clear how to model trapped foam fraction, although some models try to explain it (Kovscek et al., 1995; Cohen et al., 1997; Tang and Kovscek, 2006). The analysis presented in this paper may be applied to some trapped foam models, for instance, the model from Kovscek et al. (1995) and its derivatives.

3 The Hirasaki and Lawson's gas viscosity

The apparent gas viscosity in the presence of foam is frequently modeled by the Hirasaki and Lawson's formula

$$\mu_g = \mu_g^0 + \alpha \frac{n_f}{v_g^{1/3}}, \quad (12)$$

when foam is considered a shear-thinning fluid, where μ_g^0 is the gas viscosity in the absence of foam. The proportionality constant α depends on many factors, including the pore structure, the liquid viscosity, and the gas-liquid surface tension (Hirasaki and Lawson, 1985). Due to the inherent difficulty to obtain α , many works use it as a fitting parameter, e.g., (Chen et al., 2010; Eide et al., 2020; Kam, 2008; Kovscek et al., 1995; Simjoo and Zitha, 2015; Thorat and Bruining, 2016). Since v_g itself depends on μ_g (see (2), (3) and (10)), Eq. (12) defines μ_g implicitly, which hinders the analytical and numerical analysis of the model.

The first contribution of this work is to rewrite (12) eliminating the direct dependency on v_g . To do so, we replace (2), (3), and (10) into (12) obtaining a cubic equation in the variable $X = (k_{rg} + \lambda_w \mu_g)^{1/3}$. The resulting expression admits a unique positive root X , which can be written as

$$\mu_g = \mu_g^0 + \frac{3A}{\lambda_w} \left(\sqrt[3]{B + \sqrt{B^2 - A^3}} + \sqrt[3]{B - \sqrt{B^2 - A^3}} \right), \quad (13)$$

where

$$A := \frac{\alpha n_f \lambda_w}{3} \left(\frac{\phi(1 - S_w)}{k_{rg} |u - \lambda_w K \partial_x P_c|} \right)^{1/3} \quad \text{and} \quad B := \frac{k_{rg} + \lambda_w \mu_g^0}{2}. \quad (14)$$

Under LE conditions, the capillary pressure is constant. Therefore, term A in (13) becomes

$$A := \frac{\alpha n_{\max} n_D^{\text{LE}} \lambda_w}{3} \left(\frac{\phi(1 - S_w)}{k_{rg} |u|} \right)^{1/3}. \quad (15)$$

Since λ_w and k_{rg} are functions of S_w , and μ_g^0 , α , n_{\max} , and ϕ are constant parameters, we identify the apparent gas viscosity under LE conditions as the function $\mu_g^{\text{LE}}(S_w, n_D^{\text{LE}}, u)$.

4 Traveling wave solutions

Ashoori et al. (2011); Lozano et al. (2021) investigated traveling wave solutions for a linear kinetic Newtonian foam model, where the apparent gas viscosity (μ_g) depends only on the foam texture (n_D). Below, we present the analysis for the generic non-Newtonian model described in Section 2 with apparent viscosity formula detailed in Section 3.

4.1 Traveling wave formulation

The traveling wave solutions of a system of evolutionary PDEs are the solutions invariant to translation in space (see (Volpert et al., 2000) and references therein). Mathematically speaking, they depend on a traveling variable $\xi := x - vt$, where v is the constant wave velocity. For the system (1), (2) and (4) with step function initial conditions

$$(S_w, n_D) = \begin{cases} (S_w^-, n_D^-), & x = 0 \\ (S_w^+, n_D^+), & x > 0 \end{cases} \quad (16)$$

the traveling wave solution is represented by bounded and differentiable functions $\tilde{S}_w, \tilde{n}_D : \mathbb{R} \rightarrow \mathbb{R}$ satisfying $(\tilde{S}_w, \tilde{n}_D)(x - vt) = (S_w, n_D)(x, t)$ for a some $v \in \mathbb{R}$, all $x \in (0, L)$, $L > 0$, and all $t \in (0, +\infty)$. Moreover, the wave front $(\tilde{S}_w, \tilde{n}_D)$ must satisfy the boundary conditions (Volpert et al., 2000):

$$\lim_{\xi \rightarrow \pm\infty} (\tilde{S}_w, \tilde{n}_D)(\xi) = (S_w^\pm, n_D^\pm) \in \mathbb{R}^2, \quad \text{and} \quad \lim_{\xi \rightarrow \pm\infty} d_\xi(\tilde{S}_w, \tilde{n}_D)(\xi) = 0. \quad (17)$$

The (left) state (S_w^-, n_D^-) corresponds to the inflow boundary conditions, and the (right) state (S_w^+, n_D^+) corresponds to the initial conditions for the original PDE.

Starting from (1), (2) and (4), one may verify that the wave front $(\tilde{S}_w, \tilde{n}_D)$ is a solution of the following system of ordinary differential equations (ODEs):

$$\begin{cases} d_\xi(-v\phi\tilde{S}_w + \tilde{u}_w) = 0, \\ d_\xi[\tilde{n}_D n_{\max}(-v\phi(1 - \tilde{S}_w) + (u - \tilde{u}_w))] = \phi(1 - \tilde{S}_w)\tilde{R}, \end{cases} \quad (18)$$

for all $\xi \in \mathbb{R}$, where $\tilde{R} := R(\tilde{S}_w, \tilde{n}_D, \tilde{u}_w)$,

$$\tilde{u}_w = \frac{\lambda_w(\tilde{S}_w)}{\lambda_w(\tilde{S}_w) + \frac{k_{rg}(\tilde{S}_w)}{\tilde{\mu}_g}} \left(u + \frac{k_{rg}(\tilde{S}_w)}{\tilde{\mu}_g} K \frac{\partial P_c}{\partial S_w}(\tilde{S}_w) \frac{\partial \tilde{S}_w}{\partial \xi} \right), \quad (19)$$

and $\tilde{\mu}_g$ is given below in (23). The solution $(\tilde{S}_w, \tilde{n}_D)$ of (18) satisfying restrictions (17) is known as traveling wave solution. We can use the limits in (17) to conclude that there exists $u_g^+ := u - \lim_{\xi \rightarrow +\infty} \tilde{u}_w$ such that

$$-v\phi(1 - \tilde{S}_w) + (u - \tilde{u}_w) = -v\phi(1 - S_w^+) + u_g^+ \quad (20)$$

for all $\xi \in \mathbb{R}$. Thus, we can rewrite (18)-(19) as follows

$$\begin{cases} \frac{-\lambda_w k_{rg}}{k_{rg} + \lambda_w \tilde{\mu}_g} K \frac{\partial P_c}{\partial S_w} d_\xi \tilde{S}_w = \left[u_g^+ - \frac{k_{rg} u}{k_{rg} + \lambda_w \tilde{\mu}_g} \right] - v\phi(\tilde{S}_w - S_w^+), \\ n_{\max}(u_g^+ - v\phi(1 - S_w^+)) d_\xi \tilde{n}_D = \phi(1 - \tilde{S}_w)\tilde{R}, \end{cases} \quad (21)$$

Note that (20) also implies that, for all $\xi \in \mathbb{R}$,

$$\tilde{v}_g := \frac{|u - \tilde{u}_w|}{\phi(1 - \tilde{S}_w)} = \left| v \frac{\left(S_w^+ + \frac{u_g^+}{\phi v} \right) - \tilde{S}_w}{1 - \tilde{S}_w} \right|. \quad (22)$$

Then, one may replace (22) into (12) to obtain

$$\tilde{\mu}_g = \mu_g^0 \left(1 + \frac{\alpha n_{\max}}{\mu_g^0 |v|^{\frac{1}{3}}} \left(\frac{1 - \tilde{S}_w}{|S_w^{crit} - \tilde{S}_w|} \right)^{\frac{1}{3}} \tilde{n}_D \right), \quad (23)$$

where $S_w^{crit} := S_w^+ + u_g^+ / (v \phi)$. Equation (23) is an alternative version of (12) valid only for the traveling wave profile.

Let us summarize these calculations. The traveling wave solution of the problem (1)-(4) in the domain $(0, L) \times (0, +\infty)$, with initial condition $(S_w, n_D)(x, 0) = (S_w^+, n_D^+)$ and boundary condition $(S_w, n_D)(0, t) = (S_w^-, n_D^-)$ is given by the solution of (21) which satisfies limit conditions (17). We discuss how to obtain these limit conditions in Subsection 4.2.

The existence of the solution of (21) is not trivial. Lozano et al. (2021) investigate the existence of solutions for (21) using Newtonian foam flow and particular choice of $R = r_g - r_c$. They show that such solutions exist in specific parameter regions, depending on the model and the limit states. We do not perform such deep analysis here; however, we give evidence that the solutions exist for the examples from Section 5.

4.2 Traveling wave velocity and equilibria

The usual procedure to determine the traveling wave velocity and equilibria is to apply limits (17) to the ODE system (21). Let us assume $k_{rw}(S_w^\pm)$, $k_{rg}(S_w^\pm)$, and $d_{S_w} P_c(S_w^\pm)$ are real numbers and that $k_{rg}(S_w^\pm) > 0$. As $\lim_{\xi \rightarrow \pm\infty} d_\xi \tilde{S}_w(\xi) = 0$ from (17), it follows that $\lim_{\xi \rightarrow \pm\infty} d_x P_c(\xi) = 0$. Therefore, $\lim_{\xi \rightarrow \pm\infty} \tilde{\mu}_g(\xi) = \mu_g^{LE}(S_w^\pm, n_D^\pm, u)$. Moreover, we use the fractional flux definition in (3), and apply the limits in (17) to (19) and (21) to obtain the algebraic system of nonlinear equations

$$\frac{k_{rg}(S_w^-)}{k_{rg}(S_w^-) + \lambda_w(S_w^-) \mu_g^{LE}(S_w^-, n_D^-, u)} = f_g^-, \quad (24)$$

$$\frac{k_{rg}(S_w^+)}{k_{rg}(S_w^+) + \lambda_w(S_w^+) \mu_g^{LE}(S_w^+, n_D^+, u)} = \frac{u_g^+}{u}, \quad (25)$$

$$(u_g^+ - f_g^- u) - v \phi (S_w^- - S_w^+) = 0, \quad (26)$$

$$R(S_w^-, n_D^-, (u - u_g^+) + v \phi (S_w^- - S_w^+)) = 0, \quad (27)$$

$$R(S_w^+, n_D^+, u - u_g^+) = 0. \quad (28)$$

Most laboratory and field scale simulations use homogeneous initial saturation profiles, and measure the injection gas fractional flow to predict foam propagation. Therefore, we consider u , S_w^+ and f_g^- to be the known values and $(S_w^-, n_D^-, n_D^+, u_g^+, v)$ as the main unknowns in (24)-(28).

As discussed in Section 2, there is a particular case where the restrictions $R = 0$ and $\partial_x P_c = 0$ result in a LE foam texture $n_D = n_D^{LE}(S_w, u_w, u)$. The models from (Ashoori et al., 2011; Chen et al., 2010; Kam, 2008; Kovsky et al., 1995; Simjoo and Zitha, 2015), for instance, allow for such an expression of local-equilibrium foam texture. For these models, one may use the following strategy to solve (24)-(28) given u , S_w^+ and f_g^- :

1. Solve (24) for S_w^- using $n_D^- = n_D^{\text{LE}}(S_w^-, (1 - f_g^-)u, u)$;
2. Solve (25) for u_g^+ using $n_D^+ = n_D^{\text{LE}}(S_w^+, u - u_g^+, u)$;
3. Solve (26) for v .

This algorithm involves the solution of two uncoupled scalar nonlinear equations, which can be done either analytically or applying a classical numerical procedure, see (Mathews, 1992). After obtaining all constant parameters, one must solve the ODE system (21) with limit conditions in (17) using usual ODE solvers for nonlinear systems to obtain the traveling wave profile.

Remark. The procedure to obtain the traveling wave limits and wave velocity described above can still be used for initial gas at residual saturation. In this case, the existence of traveling wave limits rely on the following limit

$$\lim_{\xi \rightarrow +\infty} d_\xi \tilde{S}_w = \lim_{S_w \rightarrow 1 - S_{\text{gr}}} \frac{u - v \phi(1 - S_w - S_{\text{gr}})^{\frac{k_{\text{rg}} + \lambda_w \tilde{\mu}_g}{k_{\text{rg}}}}}{\lambda_w K \frac{\partial P_c}{\partial S_w}} = 0.$$

Ashoori et al. (2011) use a modified Brooks-Corey capillary pressure equation obtained by multiplying the original formula by the term $(1 - S_w - S_{\text{gr}})^c$, $c = 0.01$. Such modification does not affect the phenomenological conclusions, but guarantees the limit above holds. In the present paper, we use the model from Ashoori et al. (2011) with the referred modification. We stress that one can propose other modifications to the capillary pressure provided the limit above remains valid.

5 Application in a linear kinetics model

In this section, we apply the methodology from the previous sections to obtain traveling wave solutions for the linear kinetics foam propagation model from Ashoori et al. (2011). We use them to compare the influence of the non-Newtonian apparent viscosity in the foam model. In this model, the relative permeabilities, $k_{\text{rw}}(S_w)$ and $k_{\text{rg}}(S_w)$, are generalized Brooks-Corey expressions, fitted for the nitrogen-water flow in the Boise sandstone. The capillary pressure has an equivalent unitary pore size distribution index, also inspired in the work of Brooks and Corey (1966). Foam generation and coalescence are controlled by expressions $r_g(S_w)$ and $r_c(n_D)$ as follows

$$\begin{aligned} k_{\text{rw}}(S_w) &:= 0.2 S_{\text{we}}^{4.2}, \\ k_{\text{rg}}(S_w) &:= 0.94 (1 - S_{\text{we}})^{1.3}, \\ P_c(S_w) &:= 15000 \frac{0.022 (1 - S_w - S_{\text{gr}})^{0.01}}{S_w - S_{\text{wc}}}, \\ r_g(S_w) &:= K_c n_{\text{max}} n_D^{\text{LE}}(S_w), \\ r_c(n_f) &:= K_c n_{\text{max}} n_D, \\ n_D^{\text{LE}}(S_w) &:= \begin{cases} \tanh(400 (S_w - 0.37)) & \text{if } S_w > 0.37, \\ 0 & \text{if } S_w \leq 0.37, \end{cases} \end{aligned} \tag{29}$$

where K_c is the kinetic generation/coalescence rate parameter. The coefficient 15000 stems from the Leverett J-function (Leverett, 1941) with a gas-water surface tension of 0.03 N/m. Table 1 shows the remaining parameter values from (Ashoori et al., 2011). To summarize, we analyze the model described by (1)-(4), (12) and (29) with parameters from Table 1.

Ashoori et al. (2011) studied the incompressible foam flow considering foam as a Newtonian fluid. They used the following apparent gas viscosity formula

$$\mu_g^N := \mu_g^0 MRF^N(n_D), \quad MRF^N(n_D) = 1 + C_{MRF} n_D, \quad (30)$$

where C_{MRF} is a reference mobility reduction factor for the strongest foam. Two well-known foam properties inspired the simplification: (1) foamed gas mobility reduction is large and nearly constant at high water saturation, and (2) there exists a limiting capillary pressure, where foam collapses abruptly. Parameter α is the one that minimizes the mean squared difference between the gas mobilities under equilibrium conditions, i.e.,

$$\min_{\alpha} \int_{S_{wc}}^{1-S_{gr}} \left(\frac{k_{rg}(S_w)}{\mu_g^{LE}(S_w, n_D^{LE}(S_w), u)} - \frac{k_{rg}(S_w)}{\mu_g^0 MRF^N(n_D^{LE}(S_w))} \right)^2 dS_w. \quad (31)$$

for $u = 29.3 \mu\text{m/s}$. This mapping generalizes the one proposed by Zavala et al. (2021).

Table 1: Parameters for nitrogen and water flow in a Boise sandstone (Ashoori et al., 2011).

Property	Symbol	Value
Newtonian gas viscosity coefficient	C_{MRF}	18 500 [-]
Permeability	K	10^{-12} m^2
Kinetic parameter	K_c	200; 1; 0.01 s^{-1}
Reference foam texture	n_{\max}	$8 \times 10^{13} \text{ m}^{-3}$
Residual gas saturation	S_{gr}	0.18 [-]
Residual (connate) water saturation	S_{wc}	0.2 [-]
Total superficial velocity	u	$2.93 \times 10^{-5} \text{ m/s}$
Non-Newtonian gas viscosity coefficient	α	$2.44 \times 10^{-16} \text{ Pa s}^{\frac{2}{3}} \text{ m}^{\frac{10}{3}}$
Water viscosity	μ_w	10^{-3} Pa s
Gas viscosity in the absence of foam	μ_g^0	$2 \times 10^{-5} \text{ Pa s}$
Porosity	ϕ	0.25 [-]

In what follows, we compute traveling wave profiles for the linear kinetic model using the non-Newtonian apparent gas viscosity (12). We compare those profiles with the ones obtained using the Newtonian apparent viscosity (30). We analyze two scenarios. The first one reproduces the example found in (Ashoori et al., 2011). The second one show a case where the non-Newtonian foam model brings significant information. We also show how apparent total viscosity changes with flow velocity in the

equilibria, which helps understanding the connection between Newtonian and non-Newtonian foam models. Hereafter, the superscript ‘ N ’ identifies the properties of the Newtonian and ‘ S ’ the properties of the non-Newtonian models. Table 2 shows the equilibria computed using (24)-(28) for the Newtonian and non-Newtonian models in the two scenarios.

Table 2: Parameter values at limit states and traveling wave velocities in two scenarios used to compare Newtonian and non-Newtonian models. We use $u = 29.3\mu\text{m/s}$.

Parameter	Scenario 1 $f_w^- = 0.268; S_w^+ = 0.72$		Scenario 2 $f_w^- = 0.9; S_w^+ = 0.819$	
	Newtonian	non-Newt.	Newtonian	non-Newt.
S_w^- [-]	3.720×10^{-1}	3.719×10^{-1}	5.011×10^{-1}	4.672×10^{-1}
n_D^- [-]	6.650×10^{-1}	6.503×10^{-1}	1.000	1.000
n_D^+ [-]	1.000	1.000	1.000	1.000
u_g^+ [$\mu\text{m/s}$]	7.251×10^{-2}	6.111×10^{-3}	8.782×10^{-5}	3.193×10^{-7}
$ \nabla P ^-$ [MPa/m]	8.566	8.579	2.738	4.520
$ \nabla P ^+$ [MPa/m]	3.059×10^{-1}	3.066×10^{-1}	1.475×10^{-1}	1.475×10^{-1}
v [m/s]	2.457×10^{-4}	2.464×10^{-4}	3.687×10^{-5}	3.332×10^{-5}

5.1 Scenario 1

Scenario 1 corresponds to the flow data from the literature (Ashoori et al., 2011) with the limit states $S_w^+ = 0.72$ and $f_w^- = 0.268$. The autonomous system (21) can be rewritten in the standard form:

$$d_\xi \begin{bmatrix} \tilde{S}_w \\ \tilde{n}_D \end{bmatrix} = F(\tilde{S}_w, \tilde{n}_D); \quad \text{where}$$

$$F(S_w, n_D) := \begin{bmatrix} \left(u_g^+ - \frac{k_{rg} u}{k_{rg} + \lambda_w \mu} \right) - v \phi(S_w - S_w^+) \\ - \frac{k_{rg}}{k_{rg} + \lambda_w \mu} \lambda_w K \frac{\partial P_c}{\partial S_w} \\ \frac{\phi(1 - S_w) R}{n_{\max}(u_g^+ - v \phi(1 - S_w^+))} \end{bmatrix}$$

$$\text{and } \mu := \mu_g^0 + \frac{\alpha n_{\max}}{v^{\frac{1}{3}}} \left(\frac{1 - S_w}{|S_w^{crit} - S_w|} \right)^{\frac{1}{3}} n_D, \quad (32)$$

One standard approach for proving the existence of the solution connecting two equilibria in an autonomous system is based on the analysis of the ODE’s phase space, as done by Lozano et al. (2021). We repeat some steps of their analysis.

We start by proving that:

1. $F(S_w, n_D) = 0$ if and only if $n_D = n_D^{LE}(S_w)$ and $u_g^+ - k_{rg}/(k_{rg} + \lambda_w \mu) u = v \phi(S_w - S_w^+)$;

2. The curve $u_g^+ - k_{rg} u / (k_{rg} + \lambda_w \mu)$ restricted to $n_D = n_D^{LE}(S_w)$ intersects the straight line $v \phi(S_w - S_w^+)$ in at most two values of $S_w \in (S_{wc}, 1 - S_{gr})$.

Since $F(S_w^+, n_D^+) = F(S_w^-, n_D^-) = 0$, those are the only two roots of F in $(S_{wc}, 1 - S_{gr}) \times [0, 1]$.

Second, let us comment on the dynamics in the neighborhood of the limit states of Scenario 1 in Table 2. In two-dimensional phase space, this analysis reduces to look at the real part's sign of the eigenvalues of the Jacobian matrix $(\partial_{S_w} F, \partial_{n_D} F)$; positive signs indicate source directions, and negative signs indicate sink directions. Since $F(S_w, n_D) = 0$ only over the equilibria, the orbit (solution of (32)) exists if there is at least one source direction in the left state and at least one sink direction in the right state. Table 3 shows the eigenvalues for states $-$ and $+$ using the non-Newtonian model. In all cases, the states $-$ have eigenvalues with positive real parts (sources), and states $+$ have eigenvalues' real parts with opposite signs (saddle points), which proves existence of an orbit, i.e., traveling wave solution.

Table 3: Eigenvalues of the Jacobian matrix $(\partial_{S_w} F, \partial_{n_D} F)$ at the equilibrium states $-$ and $+$ of Scenario 1. The classification follows a typical nomenclature (Guckenheimer et al., 1984).

K_c [1/s]	State	λ_1 [1/m]	λ_2 [1/m]	Classification
200	$-$	1.089×10^5	1.715×10^6	Source
200	$+$	-1.020×10^6	8.092×10^5	Saddle
1	$-$	$1091 + 2854i$	$1091 - 2854i$	Spiral source
1	$+$	-1.020×10^6	4.046×10^3	Saddle
0.01	$-$	1.209×10^4	7.726×10^2	Source
0.01	$+$	-1.020×10^6	4.046×10^1	Saddle

Table 2 shows that the relative difference for the states n_D^- is lower than 3%, and the values of u_g^+ are approximately zero. The remaining parameter values vary less than 1% between the models. Note that the Newtonian model's values in scenario 1 coincide with those from (Ashoori et al., 2011). The solution profiles for S_w and n_D for the non-Newtonian case are very similar to the ones of the Newtonian model found in (Ashoori et al., 2011). Figure 1 shows the MRF and f_w profiles. Although the MRF we observe in the left panel of Fig. 1 a significant qualitative and quantitative change in MRF, this does not affect fractional flux curves as depicted in the right panel of the same figure.

5.2 Scenario 2

The second scenario explores higher differences between the Newtonian and non-Newtonian behaviors by taking a higher initial water saturation, $S_w^+ = 0.819$, and injecting a mixture with lower foam quality, $f_w^- = 0.9$. This scenario, usually denoted by the term low-quality regime, was not based on experimental data from the literature; it was built to enlarge the differences between Newtonian and non-Newtonian regimes describing

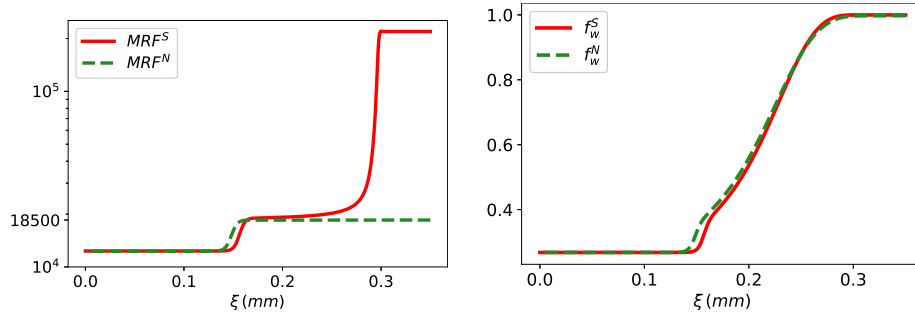


Figure 1: Mobility Reduction Factor and f_w profiles in the non-Newtonian (filled lines) and Newtonian (dashed lines) models using $K_c = 200 \text{ s}^{-1}$ in Scenario 1.

foam flow in porous media. Scenario 2 addresses a fundamental scientific discussion on understanding the non-Newtonian nature of the foam displacement. The analysis of the existence of traveling wave solutions for Scenario 2 is analogous to the one from Section 5.1 and, therefore, we omit it.

Table 2 shows the equilibria for the Newtonian and non-Newtonian models in Scenario 2. We note that the Newtonian traveling wave velocity v , water saturation S_w^- , and pressure gradient $|\nabla P|^-$ differ from the corresponding values of the non-Newtonian values 11%, 7%, and 39%, respectively. Figure 2 shows the traveling wave profiles of \tilde{S}_w and \tilde{n}_D , and the pressure gradient over the traveling wave for the non-Newtonian foam model using $K_c = 200 \text{ s}^{-1}$. Besides the difference in the limit states, the non-Newtonian foam model profiles are sharper than the ones in the Newtonian model. Figure 3 shows the MRF and f_w over the traveling wave. We use (23) to compute MRF^S . As in scenario 1, MRF is qualitatively and quantitatively different between the models. In this case, however, the fractional flux profile changes between the models leading to different water saturation profiles, see left panel of Fig. 2.

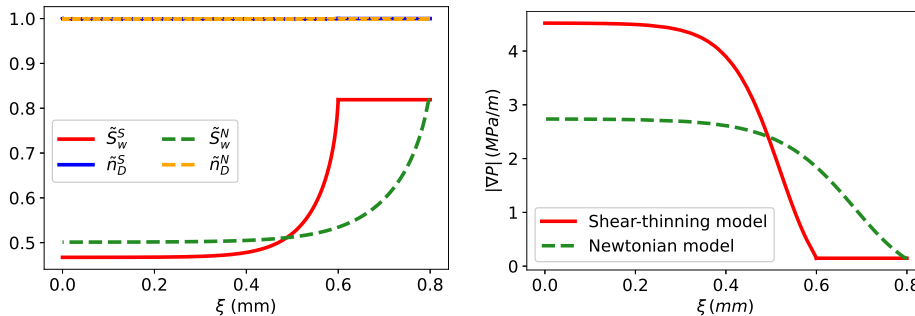


Figure 2: Wave profiles in the non-Newtonian (filled lines) and Newtonian (dashed lines) models using $K_c = 200 \text{ s}^{-1}$ in Scenario 2. Left: $\tilde{S}_w(\xi)$ and $\tilde{n}_D(\xi)$. Right: pressure gradient obtained using the formulas from Section 2.

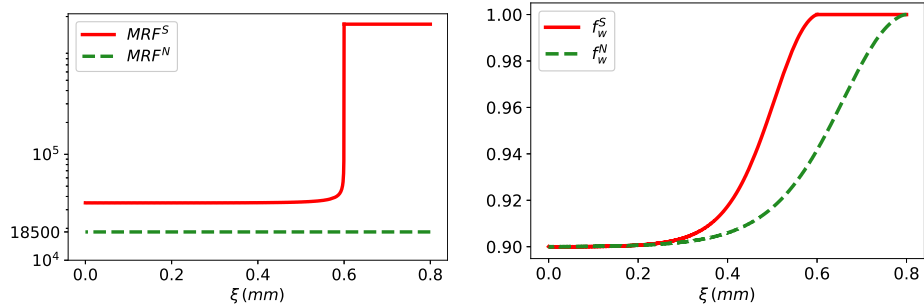


Figure 3: Mobility Reduction Factor and f_w profiles in the non-Newtonian (filled lines) and Newtonian (dashed lines) models using $K_c = 200 \text{ s}^{-1}$ in Scenario 2.

5.3 Traveling wave equilibria for different flow velocities

Figure 4 shows isolines of the superficial gas velocity u_g as a function of the foam quality f_g and the total apparent viscosity μ_{app} defined in (7). All quantities are taken considering LE conditions and $u \in [0.1 \mu\text{m/s}, 100 \mu\text{m/s}]$, a range that covers laboratory and field experimental values. One can see that the lower is the superficial gas velocity the stronger is the foam (higher μ_{app}). In agreement with (Eide et al., 2020; Gassara et al., 2020), the high-quality regime region (after the peak of the strongest foam) shrinks when the superficial gas velocity increases. In the Newtonian model, total apparent viscosity and fractional fluxes depend only on S_w , so there is a single curve for each C_{MRF} . We plot the curves $C_{MRF} = 37000$ and $C_{MRF} = 185000$ in Fig. 4 to show that one should vary C_{MRF} so that the Newtonian model better represent the non-Newtonian gas viscosity accordingly to the flow regime.

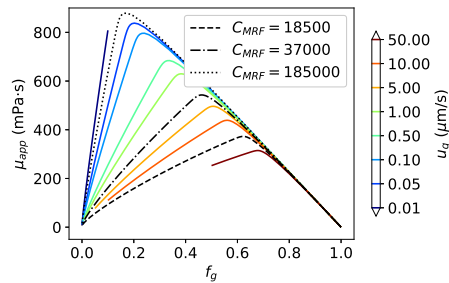


Figure 4: Apparent viscosity μ_{app} as a function of u_g and f_g , all using LE foam, for the non-Newtonian foam model. The dashed and dotted lines represent Newtonian total apparent viscosity with a given C_{MRF} .

Remark. Scenario 2 evidences some difference between the traveling wave solutions of non-Newtonian and Newtonian models. The parameter values

in this scenario assume the injection of a mixture with low gas concentration. Although it is uncommon, such configuration occurs in industrial application, e.g., surfactant alternated gas (SAG) injection in the Enhanced Oil Recovery (EOR). During this procedure, pure water (containing surfactant) and pure gas are injected into the reservoir periodically resulting in alternated low and high gas concentrations inside the porous medium.

Remark. We used the explicit Runge-Kutta method RK5(4) (Shampine, 1986) to solve (21) in the variable $\eta := -\xi$ on $(0, \eta_F)$ with initial conditions $(\tilde{S}_w, \tilde{n}_D)(0) = (S_w^+ - 10^{-6}, n_D^+)$ and time steps bounded by $\eta_F/1000$. This change of variables, ξ to $-\eta$, helps the numerical solver to find the correct solution.

6 Discussion and Conclusions

In this paper, we detailed the procedure of obtaining traveling wave solutions for a range of models describing propagation of foam in porous media. For that, we reformulate the Hirasaki and Lawson's apparent viscosity in terms of the foam model's unknowns S_w , n_D and u . We restrict the analysis to the case of constant total superficial velocity u as in previous works. It is worth mentioning that the reformulated apparent viscosity formula can be used in other contexts. One example is to reconstruct fractional fluxes directly from the experimental data.

In order to evidence the potential of the proposed methodology, we find the traveling wave solutions for the linear kinetic model from Ashoori et al. (2011). We use the solutions to quantify the importance of considering the non-Newtonian apparent viscosity in the model. We proposed a mapping procedure to map one model in the other. This procedure involves the solution of a minimization problem for the mean square difference between gas mobilities in the two models. We conclude that:

- For the cases reproduced from Ashoori et al. (2011), the non-Newtonian viscosity brings no new relevant information. This is expected in such a high-quality regime, as observed in several other works, e.g., (Cheng et al., 2000; Salazar Castillo et al., 2020; Valdez et al., 2021).
- In the low-quality example, we identify a foam flow regime with stronger non-Newtonian fluid behavior, and obtain more significant discrepancies between the two models. Our example showed a relative difference of 39% in the pressure gradient and 11% in the traveling wave velocity. Note that estimating the traveling wave velocity is crucial to predict the gas breakthrough during an enhanced recovery process in porous media. It is worth mentioning that we achieve such contrast even using the same constant total superficial velocity from Scenario 1.
- The mobility reduction factor gives significantly less information on the foam flow than the fractional flux curves. In the two scenarios we analyze, the mobility reduction factors between Newtonian and non-Newtonian presented qualitative and quantitative differences. However, the water saturation and foam texture wave profiles coin-

cide qualitatively in the first scenario, while, in the second one, they don't.

- For different total flow velocities and quality regimes, one may still use the Newtonian gas viscosity formula, although the parameters should be adjusted so that the shear-thinning behavior of foam can be accurately represented.

References

- M. M. Almajid, N. Nazari, and A. R. Kovscek. Modeling Steady-State Foam Flow: Hysteresis and Backward Front Movement. *Energy Fuels*, 33(11):11353–11363, 2019. ISSN 1520-5029. doi: 10.1021/acs.energyfuels.9b01842.
- J. M. Alvarez, H. J. Rivas, and W. R. Rossen. Unified model for steady-state foam behavior at high and low foam qualities. *SPE J.*, 6(3): 325–333, Sept. 2001. ISSN 1086-055X. doi: 10.2118/74141-PA.
- S. N. Antontsev. On the solvability of boundary value problems for degenerate two-phase porous flow equations. *Dinamika Splosnoi Sredy Vyp*, 10:28–53, 1972.
- E. Ashoori, D. Marchesin, and W. R. Rossen. Roles of transient and local equilibrium foam behavior in porous media: Traveling wave. *Colloids Surf., A*, 377(1-3):228–242, Mar. 2011. ISSN 0927-7757. doi: 10.1016/j.colsurfa.2010.12.042.
- F. R. Behenna. Acid Diversion from an Undamaged to a Damaged Core Using Multiple Foam Slugs. In *SPE - European Formation Damage Conference*, pages 441–452, 1995. ISBN 9781555634476. doi: 10.2118/30121-ms.
- F. P. Bretherton. The motion of long bubbles in tubes. *J. Fluid Mech.*, 10(2):166–188, Mar. 1961. ISSN 1469-7645. doi: 10.1017/S0022112061000160.
- R. H. Brooks and A. T. Corey. Properties of Porous Media Affecting Fluid Flow. *J. Irrig. Drain. Div.*, 92(2):61–88, 1966. ISSN 0044-7978.
- J. W. Burman and B. E. Hall. Foam As a Diverting Technique for Matrix Sandstone Stimulation. In *SPE of AIME*, Apr. 1986. doi: 10.2118/15575-ms.
- J. F. Casteel and N. F. Djabbarah. Sweep improvement in the CO₂ flooding by use of foaming agents. *SPE Reserv. Eng.*, 3(4):1186–1192, Nov. 1988. ISSN 0885-9248. doi: 10.2118/14392-PA.
- Q. Chen, M. G. Gerritsen, and A. R. Kovscek. Modeling foam displacement with the local-equilibrium approximation: Theory and experimental verification. *SPE J.*, 15(1):171–183, Mar. 2010. ISSN 1086-055X. doi: 10.2118/116735-pa.

- Z. Chen and R. E. Ewing. Fully discrete finite element analysis of multiphase flow in groundwater hydrology. *SIAM J. Numer. Anal.*, 34(6):2228–2253, Dec. 1997. ISSN 0036-1429. doi: 10.1137/S0036142995290063.
- L. Cheng, A. B. Reme, D. Shan, D. A. Coombe, and W. R. Rossen. Simulating Foam Processes at High and Low Foam Qualities. In *SPE/DOE improved oil recovery symposium*. Society of Petroleum Engineers, 2000. doi: 10.2118/59287-ms.
- D. Cohen, T. W. Patzek, and C. J. Radke. Onset of Mobilization and the Fraction of Trapped Foam in Porous Media. *Transp. Porous Media*, 28(3):253–284, 1997. ISSN 0169-3913. doi: 10.1023/A:1006552320036.
- A. T. Corey. The Interrelation Between Gas and Oil Relative Permeabilities. *Producers Monthly*, 19(1):38–41, 1954.
- A. S. de Vries and K. Wit. Rheology of gas/water foam in the quality range relevant to steam foam. *SPE Reserv. Eng.*, 5(2):185–192, 1990. ISSN 0885-9248. doi: 10.2118/18075-pa.
- Ø. Eide, M. Fernø, S. Bryant, A. Kavscek, and J. Gauteplass. Population-balance modeling of CO₂ foam for CCUS using nanoparticles. *J. Nat. Gas Sci. Eng.*, 80:103378, Aug. 2020. ISSN 1875-5100. doi: 10.1016/j.jngse.2020.103378.
- R. A. Ettinger and C. J. Radke. Influence of texture on steady foam flow in Berea sandstone. *SPE Reserv. Eng.*, 7(1):83–90, Feb. 1992. ISSN 0885-9248. doi: 10.2118/19688-PA.
- A. H. Falls, G. J. Hirasaki, T. W. Patzek, D. A. Gauglitz, D. D. Miller, and T. Ratulowski. Development of a mechanistic foam simulator: The population balance and generation by snap-off. *SPE Reserv. Eng.*, 3(3):884–892, 1988. ISSN 0885-9248. doi: 10.2118/14961-PA.
- M. A. Fernø, G. Jarand, P. Monrawee, H. Åsmund, G. Arne, A. R. Kavscek, and G. Hirasaki. Experimental study of foam generation, sweep efficiency, and flow in a fracture network. *SPE J.*, 21(4):1140–1150, Aug. 2016. ISSN 1086-055X. doi: 10.2118/170840-pa.
- O. Gassara, F. Douarche, B. Braconnier, and B. Bourbiaux. Calibrating and Scaling Semi-empirical Foam Flow Models for the Assessment of Foam-Based EOR Processes (in Heterogeneous Reservoirs). *Transp. Porous Media*, 131(1):193–221, 2020. ISSN 1573-1634. doi: 10.1007/s11242-018-01223-5.
- P. Grassia, E. Mas-Hernández, N. Shokri, S. J. Cox, G. Mishuris, and W. R. Rossen. Analysis of a model for foam improved oil recovery. *J. Fluid Mech.*, 751:346–405, 2014. doi: 10.1017/jfm.2014.287.
- J. Guckenheimer, P. Holmes, and M. Slemrod. Nonlinear Oscillations Dynamical Systems, and Bifurcations of Vector Fields. *J. Appl. Mech.*, 51(4):947–947, Dec. 1984. ISSN 0021-8936. doi: 10.1115/1.3167759.

- J. P. Heller and M. S. Kuntamukkula. Critical Review of the Foam Rheology Literature. *Ind. Eng. Chem. Res.*, 26(2):318–325, Feb. 1987. ISSN 1520-5045. doi: 10.1021/ie00062a023.
- G. J. Hirasaki and J. B. Lawson. Mechanisms of Foam Flow in Porous Media: Apparent Viscosity in Smooth Capillaries. *SPE J.*, 25(2):176–190, 1985. ISSN 0197-7520. doi: 10.2118/12129-pa.
- M. Izadi and S. I. Kam. Bubble-population-balance modeling for supercritical carbon dioxide foam enhanced-oil-recovery processes: From pore-scale to core-scale and field-scale events. *SPE Reserv. Eval. Eng.*, 22(4):1467–1480, Nov. 2019. ISSN 1094-6470. doi: 10.2118/191202-PA.
- S. A. Jones, N. Getrouw, and S. Vincent-Bonnieu. Foam flow in a model porous medium: II. the effect of trapped gas. *Soft Matter*, 14(18):3497–3503, 2018. ISSN 1744-6848. doi: 10.1039/c7sm02458d.
- S. I. Kam. Improved mechanistic foam simulation with foam catastrophe theory. *Colloids Surf., A*, 318(1-3):62–77, 2008. ISSN 0927-7757. doi: 10.1016/j.colsurfa.2007.12.017.
- S. I. Kam, Q. P. Nguyen, Q. Li, and W. R. Rossen. Dynamic simulations with an improved model for foam generation. *SPE J.*, 12(1):35–48, Mar. 2007. ISSN 1086-055X. doi: 10.2118/90938-PA.
- H. Kharabaf and Y. C. Yortsos. Pore Network Model for Foam Formation and Propagation in Porous Media. *SPE J.*, 3(1):42–53, Mar. 1998. ISSN 1086-055X. doi: 10.2118/36663-pa.
- A. R. Kovscek, T. W. Patzek, and C. J. Radke. A mechanistic population balance model for transient and steady-state foam flow in Boise sandstone. *Chem. Eng. Sci.*, 50(23):3783–3799, 1995. ISSN 0009-2509. doi: 10.1016/0009-2509(95)00199-F.
- M. C. Leverett. Capillary Behavior in Porous Solids. *Trans. AIME*, 142(01):152–169, 1941. ISSN 0081-1696. doi: 10.2118/941152-g.
- K. Li and R. N. Horne. Comparison of methods to calculate relative permeability from capillary pressure in consolidated water-wet porous media. *Water Resour. Res.*, 42(6):1–9, June 2006. ISSN 0043-1397. doi: 10.1029/2005WR004482.
- L. F. Lozano, R. Q. Zavala, and G. Chapiro. Mathematical properties of the foam flow in porous media. *Comput. Geosci.*, 25(1):515–527, Feb. 2021. ISSN 1420-0597. doi: 10.1007/s10596-020-10020-3.
- S. S. Marsden and S. A. Khan. The Flow of Foam Through Short Porous Media And Apparent Viscosity Measurements. *SPE J.*, 6(01):17–25, Mar. 1966. ISSN 0197-7520. doi: 10.2118/1319-pa.
- J. H. Mathews. *Numerical Methods For Mathematics, Science, and Engineering*. Prentice-Hall International, Englewood Cliffs, N.J, 1992. ISBN 0136249906. doi: 10.2307/2282127.

- T. W. Patzek. Description of Foam Flow in Porous Media by the Population Balance Method. In *ACS Symposium Series*, volume 373, pages 326–341. ACS, July 1988. doi: 10.1021/bk-1988-0373.ch016.
- W. R. Rossen. Rheology of foam in porous media at the "limiting capillary pressure. In *6th European Symposium on IOR*. EAGE, 1991. doi: 10.3997/2214-4609.201411236.
- R. O. Salazar Castillo, S. F. Ter Haar, C. G. Ponnens, M. Bos, and W. Rossen. Fractional-Flow Theory for Non-Newtonian Surfactant-Alternating-Gas Foam Processes. *Transp. Porous Media*, 131(2):399–426, jan 2020. ISSN 0169-3913. doi: 10.1007/s11242-019-01351-6.
- L. F. Shampine. Some practical Runge-Kutta formulas. *Math. Comp.*, 46(173):135–135, Jan. 1986. ISSN 0025-5718. doi: 10.1090/s0025-5718-1986-0815836-3.
- M. Simjoo and P. L. J. Zitha. Modeling of Foam Flow Using Stochastic Bubble Population Model and Experimental Validation. *Transp. Porous Media*, 107(3):799–820, Apr. 2015. ISSN 0169-3913. doi: 10.1007/s11242-015-0468-y.
- G. Q. Tang and A. R. Kavscek. Trapped gas fraction during steady-state foam flow. *Transp. Porous Media*, 65(2):287–307, Nov. 2006. ISSN 0169-3913. doi: 10.1007/s11242-005-6093-4.
- R. Thorat and H. Bruining. Foam Flow Experiments. I. Estimation of the Bubble generation-Coalescence Function. *Transp. Porous Media*, 112(1):53–76, 2016. ISSN 1573-1634. doi: 10.1007/s11242-016-0632-z.
- A. R. Valdez, B. M. Rocha, J. M. F. Façanha, A. V. O. de Souza, A. Perez-Gramatges, G. Chapiro, and R. W. Santos. Foam-assisted water–gas flow parameters: From core-flood experiment to uncertainty quantification and sensitivity analysis. *Transp. Porous Media*, pages 1–21, 2021.
- M. T. van Genuchten. A Closed-form Equation for Predicting the Hydraulic Conductivity of Unsaturated Soils. *Soil Sci. Soc. Am. J.*, 44(5):892–898, 1980. ISSN 1435-0661. doi: 10.2136/sssaj1980.03615995004400050002x.
- F. Vassenden and T. Holt. Experimental Foundation for Relative Permeability Modeling of Foam. In *SPE/DOE IOR Symposium*. SPE, 1998. doi: 10.2118/39660-ms.
- A. I. Volpert, V. A. Volpert, and V. A. Volpert. *Translations of Mathematical Monographs- Traveling Wave Solutions of Parabolic Systems*, volume 140. AMS, 2000. ISBN 0821897578.
- R. Q. Zavala, L. F. Lozano, G. Chapiro, and P. L. J. Zitha. Analytical solution for the population-balance model describing foam displacement. *Transport in Porous Media*, -:1–17, 2021. doi: 10.1007/s11242-021-01589-z.

P. L. J. Zitha. A new stochastic bubble population model for foam in porous media. In *Proceedings - SPE Symposium on IOR*, volume 1, pages 116–129. SPE, 2006. doi: 10.2118/98976-ms.